New results on Mesonic Weak Decay of p-shell Λ-Hypernuclei

The FINUDA Collaboration

M. Agnello [a,b], A. Andronenkov [c], G. Beer [d], L. Benussi [e], M. Bertani [e],
H.C. Bhang [f], G. Bonomi [g,h], E. Botta [i,b,1], M. Bregant [j,k], T. Bressani [i,b],
S. Bufalino [i,b], L. Busso [ℓ,b], D. Calvo [b], P. Camerini [j,k], B. Dalena [m,c],
F. De Mori [i,b], G. D'Erasmo [m,c], F.L. Fabbri [e], A. Feliciello [b], A. Filippi [b],
E.M. Fiore [m,c], A. Fontana [h], H. Fujioka [n], P. Genova [h], P. Gianotti [e],
N. Grion [k], O. Hartmann [e], B. Kang [f], V. Lenti [m], V. Lucherini [e],
S. Marcello [i,b], T. Maruta [o], N. Mirfakhrai [p], P. Montagna [q,h], O. Morra [r,b],
T. Nagae [n], D. Nakajima [s], H. Outa [t], E. Pace [e], M. Palomba [c],
A. Pantaleo [c], A. Panzarasa [h], V. Paticchio [c], S. Piano [k], F. Pompili [e],
R. Rui [j,k], A. Sanchez Lorente [u], M. Sekimoto [v], G. Simonetti [m,c],
A. Toyoda [v], R. Wheadon [b], A. Zenoni [g,h]

and

A. Gal [w]

[a] *Dipartimento di Fisica, Politecnico di Torino, Corso Duca degli Abruzzi 24, Torino, Italy*
[b] *INFN Sezione di Torino, via P. Giuria 1, Torino, Italy*
[c] *INFN Sezione di Bari, via Amendola 173, Bari, Italy*
[d] *University of Victoria, Finnerty Rd., Victoria, Canada*
[e] *Laboratori Nazionali di Frascati dell'INFN, via. E. Fermi, 40, Frascati, Italy*
[f] *Department of Physics, Seoul National University, 151-742 Seoul, South Korea*
[g] *Dipartimento di Meccanica, Universita' di Brescia, via Valotti 9, Brescia, Italy*
[h] *INFN Sezione di Pavia, via Bassi 6, Pavia, Italy*
[i] *Dipartimento di Fisica Sperimentale, Universita' di Torino, Via P. Giuria 1, Torino, Italy*
[j] *Dipartimento di Fisica, Universita' di Trieste, via Valerio 2, Trieste, Italy*
[k] *INFN Sezione di Trieste, via Valerio 2, Trieste, Italy*
[ℓ] *Dipartimento di Fisica Generale, Universita' di Torino, Via P. Giuria 1, Torino, Italy*
[m] *Dipartimento di Fisica Universita' di Bari, via Amendola 173, Bari, Italy*
[n] *Department of Physics, Kyoto University, Sakyo-ku, Kyoto Japan*
[o] *Department of Physics, Tohoku University, Sendai 980-8578, Japan*
[p] *Department of Physics, Shahid Behesty University, 19834 Teheran, Iran*
[q] *Dipartimento di Fisica Teorica e Nucleare, Universita' di Pavia, via Bassi 6, Pavia, Italy*
[r] *INAF-IFSI, Sezione di Torino, Corso Fiume 4, Torino, Italy*
[s] *Department of Physics, University of Tokyo, Bunkyo, Tokyo 113-0033, Japan*
[t] *RIKEN, Wako, Saitama 351-0198, Japan*
[u] *Institüt fur Kernphysik, Johannes Gutenberg-Universität Mainz, Germany*

[v] *High Energy Accelerator Research Organization (KEK), Tsukuba, Ibaraki 305-0801, Japan*
[w] *Racah Institute of Physics, The Hebrew University, Jerusalem 91904, Israel*

Abstract

The FINUDA experiment performed a systematic study of the charged mesonic weak decay channel of p-shell Λ-hypernuclei. Negatively charged pion spectra from mesonic decay were measured with magnetic analysis for the first time for $^{7}_{\Lambda}$Li, $^{9}_{\Lambda}$Be, $^{11}_{\Lambda}$B and $^{15}_{\Lambda}$N. The shape of the π^{-} spectra was interpreted through a comparison with pion distorted wave calculations that take into account the structure of both hypernucleus and daughter nucleus. Branching ratios $\Gamma_{\pi^{-}}/\Gamma_{tot}$ were derived from the measured spectra and converted to π^{-} decay rates $\Gamma_{\pi^{-}}$ by means of known or extrapolated total decay widths Γ_{tot} of p-shell Λ-hypernuclei. Based on these measurements, the spin-parity assignment $1/2^{+}$ for $^{7}_{\Lambda}$Li and $5/2^{+}$ for $^{11}_{\Lambda}$B ground-state are confirmed and a spin-parity $3/2^{+}$ for $^{15}_{\Lambda}$N ground-state is assigned for the first time.

Key words: p-shell Λ-hypernuclei, mesonic decay, ground-state spin assignment
PACS: 21.80.+a, 13.75.Ev

1. Introduction

A Λ-hypernucleus in its ground-state decays to non-strange nuclear systems through the mesonic (MWD) and non-mesonic (NMWD) weak decay mechanisms. In MWD the Λ hyperon decays to a nucleon and a pion in the nuclear medium, similarly to the weak decay mode in free space:

$$\Lambda_{free} \rightarrow p + \pi^{-} + 37.8 \text{ MeV} \quad (64.2\%) \tag{1}$$

$$n + \pi^{0} + 41.1 \text{ MeV} \quad (35.8\%) \tag{2}$$

in which the emitted nucleon (pion) carries a momentum $q \approx 100$ MeV/c. For a Λ-hypernucleus, the total decay width (or equivalently the decay rate) $\Gamma_{tot}(^{A}_{\Lambda}Z)$ is given by the sum of the mesonic decay width (Γ_{m}) and the non-mesonic decay width (Γ_{nm}), where the first term can be further expressed as the sum of the decay widths for the emission of negative ($\Gamma_{\pi^{-}}$) and neutral ($\Gamma_{\pi^{0}}$) pions:

$$\Gamma_{tot}(^{A}_{\Lambda}Z) = \Gamma_{\pi^{-}} + \Gamma_{\pi^{0}} + \Gamma_{nm}, \tag{3}$$

with $\Gamma_{tot}(^{A}_{\Lambda}Z)$ expressed in terms of the hypernuclear lifetime as:

$$\Gamma_{tot}(^{A}_{\Lambda}Z) = \hbar/\tau(^{A}_{\Lambda}Z). \tag{4}$$

MWD is suppressed in hypernuclei with respect to the free-space decay due to the Pauli principle, since the momentum of the emitted nucleon is by far smaller than the nuclear Fermi momentum ($k_{F} \simeq 270$ MeV/c) in all nuclei except for the lightest, s-shell ones.

---

[1] Corresponding author. Fax: +39 011 6707324; e-mail address: botta@to.infn.it

The theory of hypernuclear MWD was initiated by Dalitz [1,2], based on a phenomenological Lagrangian describing the elementary decay processes (1) and (2), and motivated by the observation of MWD reactions in the pioneering hypernuclear physics experiments with photographic emulsions that provided means of extracting hypernuclear ground-state spins and parities; see Ref. [3] for a recent summary. Following the development of counter techniques for use in (K^-, π^-) and (π^+, K^+) reactions in the 1970s and 1980s, a considerable body of experimental data on Γ_{π^-} and/or Γ_{π^0} is now available on light Λ-hypernuclei up to $^{12}_{\Lambda}C$: $^{4}_{\Lambda}H$ [4], $^{4}_{\Lambda}He$ [5], $^{5}_{\Lambda}He$ [6], $^{11}_{\Lambda}B$ and $^{12}_{\Lambda}C$ [6–9].

Comprehensive calculations of the main physical entities of MWD were performed during the 1980s and 1990s for very light s-shell [10,11], p-shell [11–13] and sd-shell hypernuclei [11,13]. The basic ingredients of the calculations are the Pauli suppression effect, the enhancement of MWD owing to the pion-nuclear polarization effect in the nuclear medium as predicted for MWD in Refs. [14,15], the sensitive final-state shell-structure dependence, and the resulting charge dependence of the decay rates.

An important ingredient of MWD calculations is the choice of pion-nucleus potential which generates pion-nuclear distorted waves that strongly affect the magnitude of the pionic decay rates. Indeed, for low-energy pions, the pion-nucleus potential has been studied so far through π-nucleus scattering experiments [16] and measurements of X-rays from pionic atoms [17]; the study of MWD in which a pion is created by the decay of a Λ hyperon deep inside the nucleus offers important opportunities to investigate in-medium pions and to discriminate between different off-shell extrapolations inherent in potential models. For this reason MWD continues to be an interesting item of hypernuclear physics, and precise and systematic determinations of Γ_{π^-} and Γ_{π^0} are very welcome.

In the present work we report on new measurements by the FINUDA experiment of MWD of hypernuclei in the p-shell, comparing the measured π^- spectra and decay rates with the calculations by one of the authors [18] that update the calculations by Motoba $et\ al.$ [11–13]. These two sets of spectroscopic calculations agree reasonably well with each other for all hypernuclei considered in the present report, except for $^{15}_{\Lambda}N$ which is discussed in detail below. The measured spectra are consistent with the observation, made in these shell-model calculations, that the partial decay contributions from the high-lying continuum of the daughter nuclear system outside the $0\hbar\omega$ p-shell configuration are unimportant in this mass range. The level of agreement between the reported measurements and the calculations allows us to confirm the previous spin-parity assignments made for $^{7}_{\Lambda}Li$ and $^{11}_{\Lambda}B$, and to establish a new assignment, $J^\pi = 3/2^+$, for $^{15}_{\Lambda}N$ ground-state.

2. Experimental and analysis techniques

FINUDA is a hypernuclear physics experiment, with cylindrical symmetry, installed at one of the two interaction regions of the $DA\Phi NE$ e^+e^- collider, the INFN-LNF Φ-factory. A description of the experimental apparatus can be found in [19,20]. Here we briefly sketch its main components, moving outwards from the beam axis: the *interaction/target region*, composed by a barrel of 12 thin scintillator slabs (TOFINO), surrounded by an octagonal array of Si microstrips (ISIM) facing eight target tiles; the *external tracking device*, consisting of four layers of position sensitive detectors (a decagonal array of Si microstrips (OSIM), two octagonal layers of low mass drift chambers

(LMDC) and a stereo system of straw tubes (ST)) arranged in coaxial geometry; the *external time of flight detector* (TOFONE), a barrel of 72 scintillator slabs. The whole apparatus is placed inside a uniform 1.0 T solenoidal magnetic field; the tracking volume is immersed in He atmosphere to minimize the multiple scattering effect.

The scientific program of the experiment is focussed on the study of spectroscopy and decay of Λ-hypernuclei produced by means of the (K^-, π^-) reaction with K^-'s at rest:

$$K_{stop}^- + {}^A\text{Z} \to \pi^- + {}^A_\Lambda\text{Z} \tag{5}$$

by stopping in very thin targets the low energy (~ 16 MeV) K^-'s coming from the $\Phi \to K^- K^+$ decay channel. In (5) ${}^A\text{Z}$ indicates the target nucleus and ${}^A_\Lambda\text{Z}$ the produced Λ-hypernucleus. Λ-hypernuclei decay through both the mesonic weak decay processes:

$$\begin{aligned}
{}^A_\Lambda\text{Z} &\to {}^A(\text{Z}+1) + \pi^- \tag{6}\\
{}^A_\Lambda\text{Z} &\to {}^A\text{Z} + \pi^0 \tag{7}
\end{aligned}$$

and the non-mesonic weak decay processes:

$$\begin{aligned}
{}^A_\Lambda\text{Z} &\to {}^{A-2}(\text{Z}-1) + p + n \tag{8}\\
{}^A_\Lambda\text{Z} &\to {}^{A-2}\text{Z} + n + n \tag{9}
\end{aligned}$$

where the final nuclear states in (6-9) are not necessarily particle stable. In contrast to the mesonic decays, the non-mesonic decays are not Pauli blocked, producing high-momentum nucleons (≤ 600 MeV/c).

The thinness of the target materials needed to stop the K^-'s, the high transparency of the FINUDA tracker and the very large solid angle ($\sim 2\pi$ sr) covered by the detector ensemble make the FINUDA apparatus suitable to study the formation and the decay of Λ-hypernuclei by means of high resolution magnetic spectroscopy of the charged particles emitted in the processes (5) [19], (6) and (8) [21]; the features of the apparatus give also the possibility to investigate many other final states produced in the interaction of stopped kaons with nuclei [22].

In this paper results are presented obtained by analyzing the data collected by the FINUDA experiment from 2003 to 2007 with a total integrated luminosity of 1156 pb^{-1}. Only targets leading to the formation of the p-shell hypernuclei ${}^7_\Lambda\text{Li}$, ${}^9_\Lambda\text{Be}$, ${}^{11}_\Lambda\text{B}$ and ${}^{15}_\Lambda\text{N}$ are here considered, namely ${}^7\text{Li}$ (2×, 4 mm thick, natural isotopic composition), ${}^9\text{Be}$ (2×, 2 mm thick, natural isotopic composition), ${}^{12}\text{C}$ (3×, 1.7 mm thick, natural isotopic composition, mean density 2.265 g cm^{-3}) and D_2O (mylar walled, 1×, 3 mm thick), together with ${}^6\text{Li}$ targets (2×, 4 mm thick, 90% enriched) leading to the production of ${}^5_\Lambda\text{He}$; ${}^5_\Lambda\text{He}$ is reported for the sake of completeness.

To investigate the MWD process (6) events where analyzed in which two π^-'s were detected in coincidence. One π^-, with a momentum as high as $260 - 290$ MeV/c, gives the signature of the formation of the ground-state of the hypernuclear system or of a low lying excited state decaying to it by electromagnetic emission. The second π^-, with a momentum lower than 115 MeV/c, gives the signature of the decay. By requiring this coincidence, negative pions are the only negative particles originating from the K^-'s stopping point in the targets that enter the tracking volume of the apparatus. Nevertheless, to get a cleaner data sample, only tracks identified as π^-'s by the FINUDA detectors were considered. In particular, the information of the specific energy loss in

4

both OSIM and the LMDC's and the mass identification from the time of flight system (TOFINO-TOFONE), if present, were used to obtain a multiple identification selection.
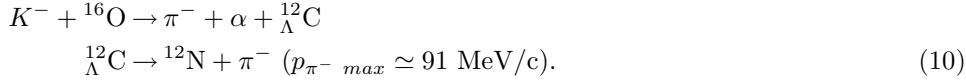
In the present analysis we required good quality tracks to determine the momentum of the formation π^-. These tracks must originate in a properly defined fiducial volume around the primary K^- vertex and are identified by four hits, one in each of the FINUDA tracking detectors (*long tracks*), and are selected with a quite strict requirement on the χ^2 from the track fitting procedure (corresponding to a 90% confidence level). They have a resolution $\Delta p/p \sim 1\%$ FWHM in the region $260-280$ MeV/c; this resolution is about twice worse than the best value obtained with top quality tracks [19] for spectroscopy studies. The worsening was due to the more relaxed quality criteria applied to increase the statistics of the sample available for the coincidence measurement. In particular, no cut has been made to select the direction of the outgoing tracks.

target ^{A}Z	final hypernucleus	p_{π^-} (MeV/c)	B.E. ($^A_\Lambda$Z) (MeV)	references
^{6}Li	$^5_\Lambda$He	$272 - 278$	$0.63 - 5.99$	[6,23]
^{7}Li	$^7_\Lambda$Li	$273 - 279$	$1.85 - 7.45$	[24–26]
^{9}Be	$^9_\Lambda$Be	$280 - 286$	$1.50 - 7.00$	[24,25,27,28]
^{12}C	$^{11}_\Lambda$B	$258 - 264$	$-2.00 - 2.75$	[28,29,19]
^{12}C	$^{12}_\Lambda$C	$267 - 273$	$9.00 - 14.00$	[28,29,19]
^{16}O	$^{15}_\Lambda$N	$265 - 270.5$	$0.0 - 4.90$	[28,25]
^{16}O	$^{16}_\Lambda$O	$270.5 - 282$	$4.90 - 15.40$	[28,25]

Table 1
Summary of the momentum and binding energy (B.E.) intervals selected to identify the formation of various hypernuclear systems. First column: target nucleus ^{A}Z; second column: weakly decaying final hypernucleus; third column: production-pion momentum interval; fourth column: $^A_\Lambda$Z binding energy interval; fifth column: references to previous missing mass spectroscopy experiments.

Table 1 reports the binding energy intervals selected to identify the formation of the different hypernuclei. The intervals have been determined by comparing our experimental inclusive formation spectra with the known values of binding energies for ground-states and low lying excited states, as deduced from the references indicated in the last column. The interval width takes into account our experimental resolution, $\sigma_p \sim 1$ MeV/c and $\sigma_{B.E.} \sim 1$ MeV for a typical pion momentum of about 270 MeV/c. For $^7_\Lambda$Li a sharp cut was set at an excitation energy of 3.94 MeV, corresponding to the threshold for the $^7_\Lambda$Li $\to$ $^5_\Lambda$He $+ d$ fragmentation. As it is well known, for $^{11}_\Lambda$B and $^{15}_\Lambda$N, produced on ^{12}C and ^{16}O (D$_2$O) targets respectively, the production momentum region *partially* overlaps the higher part of the momentum spectrum of π^-'s emitted in the Λ quasi-free (Λ_{qf}) production. This holds particularly for $^{15}_\Lambda$N which is expected to be dominantly formed by proton emission from the two peaks of $^{16}_\Lambda$O observed at B.E.$\simeq 2$ MeV and B.E.$\simeq -4$ MeV [30]. However, in order to minimize the contamination in the $^{15}_\Lambda$N decay spectrum by decays of other hypernuclear species, which may be formed in the opening of higher energy emission channels, events were selected corresponding only to the positive B.E. $^{16}_\Lambda$O peak, as indicated in Table 1. A likely source of contamination is provided by the production of $^{12}_\Lambda$C and its subsequent mesonic decay:

$$K^- + {}^{16}\mathrm{O} \rightarrow \pi^- + \alpha + {}^{12}_{\Lambda}\mathrm{C}$$
$${}^{12}_{\Lambda}\mathrm{C} \rightarrow {}^{12}\mathrm{N} + \pi^- \quad (p_{\pi^-\ max} \simeq 91 \text{ MeV/c}). \tag{10}$$

For ${}^{11}_{\Lambda}\mathrm{B}$, on the other hand, it was enough to focus on the sizable excitation peak of ${}^{12}_{\Lambda}\mathrm{C}$ at B.E.$\simeq 0$ MeV which is known to lead, upon proton emission, to several excited states of ${}^{11}_{\Lambda}\mathrm{B}$ [31].
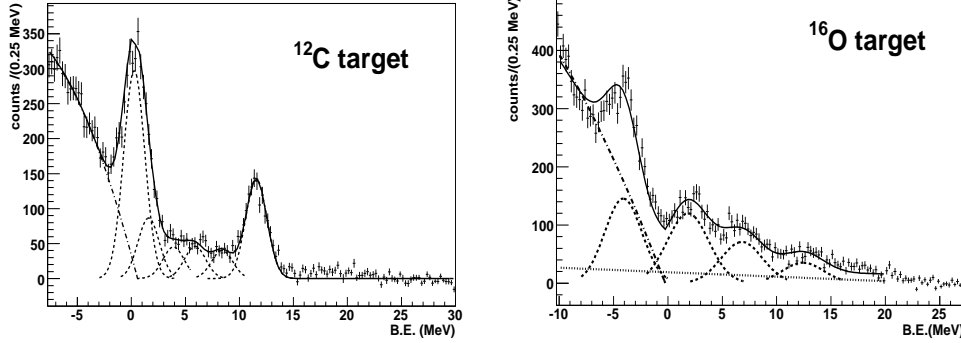

Fig. 1. Inclusive binding energy spectra for good quality π^- tracks coming from ${}^{12}\mathrm{C}$ (left) and ${}^{16}\mathrm{O}$ (right) targets. The continuous line is the best fit curve to the spectra; the dashed curves represent the contributions from the known hypernuclear states and the dot-dashed curve the Λ_{qf} background. For ${}^{16}\mathrm{O}$ the dotted curve parametrizes the K^- decay in flight.

Moreover, it should be noted that the contribution to the inclusive spectra due to the reaction chain:

$$K^- + (np) \rightarrow \Sigma^- + p \qquad \Sigma^- \rightarrow n + \pi^- \tag{11}$$
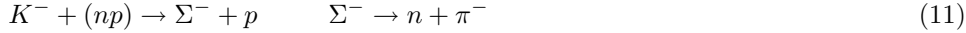
constitutes the only physical background below the hypernuclear formation peaks. It was evaluated by simulating a sample of background events and applying to the simulated data the same selection criteria as for the real ones. The background spectra were then normalized to the experimental ones above the kinematical limits for the hypernuclear ground-state formation and subtracted. A detailed description of such a procedure is available in Ref. [21].

Figure 1 shows the inclusive binding energy spectra for formation π^- from ${}^{12}\mathrm{C}$ and ${}^{16}\mathrm{O}$ targets, after subtraction of the $K^-(np)$ background. The continuous line is the best fit to the spectra, while the dashed curves represent the contributions from the known hypernuclear states and the dot-dashed curve represents the polynomial background, due to Λ_{qf} production in the negative B.E. region. In the positive B.E. region a background contribution from K^-'s decay in flight, shown separately in the figure for ${}^{16}\mathrm{O}$, is also considered. This background affects differently the targets placed in different positions with respect to the e^+e^- interaction region due to the fact that the (e^+, e^-) crossing beams collide with an angle of 12.5 mrad in order to increase the luminosity; the effect has been very well studied in [20]. On the other hand, this background affects only the inclusive B.E. spectra and does not give any contribution to the low energy π^- spectra from MWD, for which a two π^- coincidence is required.

6

Table 2 reports the binding energy values of the hypernuclear states obtained from the global fitting procedure in the B.E. regions indicated in Table 1, as mean values of the corresponding gaussians; the χ^2/ndf values are also indicated. It must be noted that these binding energy values can be different from the ones obtained in analyses dedicated to spectroscopy studies, due to the relaxation of the quality cuts applied to the tracks: indeed, the requirement of the coincidence with a low momentum π^- acts as a filter that allows to untighten the quality selections on the long tracks, as will be shown in the next section. The precise choice of peaks does not change the MWD spectra at any qualitative level, except for reducing the sample statistics.

peak		$^{7}_{\Lambda}$Li (MeV)	$^{9}_{\Lambda}$Be (MeV)	$^{12}_{\Lambda}$C (MeV)	$^{16}_{\Lambda}$O (MeV)
1 g.s.	B.E.	5.85 ± 0.13	6.30 ± 0.10	11.57 ± 0.04	12.42 fixed
2	B.E	3.84 ± 0.15	3.45 ± 0.10	8.4 fixed	6.800 ± 0.017
3	B.E.	1.9 ± 0.3	0.25 ± 0.22	5.9 fixed	1.85 fixed
4	B.E	0.39 ± 0.20		3.9 fixed	-4.100 ± 0.004
5	B.E	-2.000 ± 0.047		1.6 fixed	
6	B.E			0.27 fixed	
	χ^2/ndf	1.10	1.00	1.72	1.78

Table 2
Mean values of the gaussians representing hypernuclear states in global best fits to binding energy inclusive spectra for $^{7}_{\Lambda}$Li, $^{9}_{\Lambda}$Be, $^{12}_{\Lambda}$C and $^{16}_{\Lambda}$O: only the peaks contributing to the B.E. selections of Table 1 are considered. The FWHM of the peaks for $^{7}_{\Lambda}$Li, $^{9}_{\Lambda}$Be and $^{12}_{\Lambda}$C is 2.31 MeV, while for $^{16}_{\Lambda}$O is 4.48 MeV, due to the malfunctioning of the outer drift chamber directly facing the target. Values of χ^2/ndf for global fits (hypernuclear states and polynomial background) are also reported. See the references in the fifth column of Table 1 for comparison with previous measurements.

For the decay π^- momentum measurement only tracks not reaching the ST system (*short tracks*) have been used. The lower threshold for the detection momentum of these π^-'s is ~ 80 MeV/c. These tracks correspond mainly to particles *backward emitted* from the targets, crossing the whole interaction/target region before entering the tracker; their momentum resolution is $\Delta p/p \sim 6\%$ FWHM at 110 MeV/c.

The acceptance for low energy π^-'s, ϵ, was evaluated for each target, taking into account the geometrical layout, the efficiency of the FINUDA pattern recognition algorithm, the trigger and the efficiency of the quality cuts applied in the analysis procedure. The acceptance function, $R = 1/\epsilon$, for the momentum features a negative quadratic exponential behaviour in the $80 - 160$ MeV/c range and flattens above 90 MeV/c; for the kinetic energy the behaviour is similar in the $20 - 70$ MeV range, as shown in Fig. 2 for $^{7}_{\Lambda}$Li with a dot-dashed line. The error on the acceptance function is always $< 5\%$.

3. MWD π^-'s spectra

It is worth recalling that the information available up to now on the charged MWD of light hypernuclei consists almost entirely of $\Gamma_{\pi^-}/\Gamma_\Lambda$ values obtained by means of counting measurements in coincidence with the hypernuclear formation π^- detection, with no magnetic analysis of the decay meson; π^- kinetic energy spectra have been

obtained for $^{12}_{\Lambda}$C MWD only [9]. The π^- spectra presented here allow to have a more careful confirmation of the elementary mechanism that is supposed to underlie the decay process, as well as to have information on the spin-parity of the initial hypernuclear ground state. In this respect the study of pion spectra from MWD can be regarded as an indirect spectroscopic investigation tool.

Due to the π^- momentum detection threshold of the apparatus ($\sim$ 80 MeV/c), only MWD spectra of $^{7}_{\Lambda}$Li, $^{9}_{\Lambda}$Be, $^{11}_{\Lambda}$B (^{12}C targets) and $^{15}_{\Lambda}$N (^{16}O target) were investigated. Spectra from $^{12}_{\Lambda}$C and $^{16}_{\Lambda}$O could not be observed.

Background coming from Λ_{qf} decay was simulated and subtracted from the $^{11}_{\Lambda}$B spectrum, by normalizing the area of the simulated spectra, after reconstruction, to the experimental ones in the $110-160$ MeV/c decay-pion region. Each spectrum was corrected by means of the acceptance function, R, described in the previous section. The decay π^- momentum spectra show interesting structures whose meaning can be better understood by considering the corresponding kinetic energy spectra that are directly related to the excitation function of the daugther nucleus. Kinetic energy spectra, background subtracted and acceptance corrected, were evaluated for MWD of $^{7}_{\Lambda}$Li, $^{9}_{\Lambda}$Be, $^{11}_{\Lambda}$B and $^{15}_{\Lambda}$N.
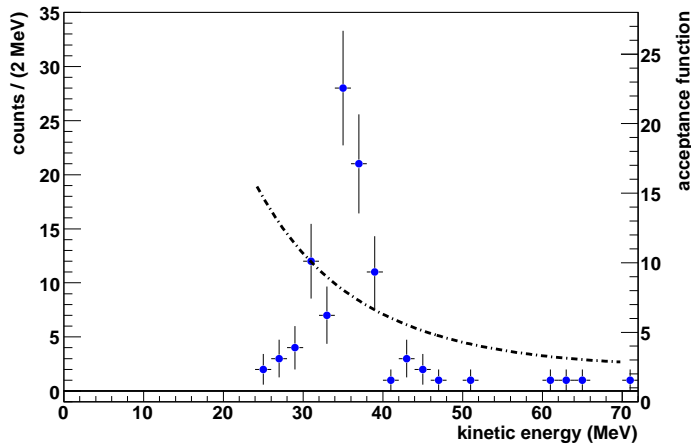

Fig. 2. Kinetic energy spectrum of MWD π^- for $^{7}_{\Lambda}$Li before acceptance correction. The dot-dashed curve is the acceptance function, R, to be applied to the data.

In Fig. 2, the kinetic energy spectrum for $^{7}_{\Lambda}$Li, before applying the acceptance correction, is reported. The acceptance correction is represented by the dot-dashed curve. The errors are statistical only. It is evident that the low energy π^- spectrum is practically background free and that the $50-70$ MeV contribution is negligible and compatible with zero. This demonstrates the effectiveness of the coincidence requirement. The small residual background, which is similar also for the other targets, has been evaluated after acceptance correction and subtracted to calculate the decay ratio (see next section). In the following only the $16-60$ MeV region of the MWD spectra will be shown.
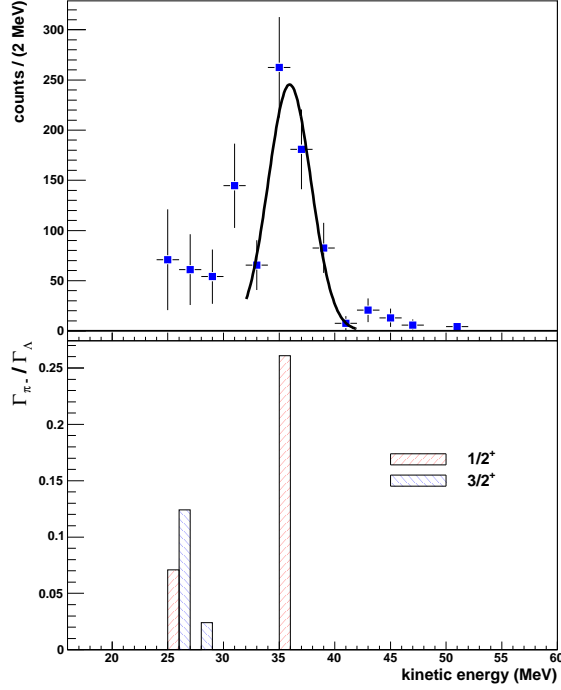
8

Fig. 3. Upper part: kinetic energy spectrum of MWD π^- for $^7_\Lambda$Li after acceptance correction. The solid curve is a gaussian fit to the peak in the spectrum, to compare with theoretical predictions in the lower part. Lower part: calculated major decay rates to final ^{7}Be states from [18], in red bars for $^7_\Lambda$Li ground-state spin-parity $1/2^+$, and in blue bars for $^7_\Lambda$Li ground-state spin-parity $3/2^+$ (see text)

.

3.1. $^7_\Lambda$Li

In Fig. 3 the acceptance corrected spectrum for $^7_\Lambda$Li is shown in the upper part and compared with calculated decay ratios ($\Gamma_{\pi^-}/\Gamma_\Lambda$) to final ^{7}Be states [18] shown in the lower part. These calculated rates are close to those calculated by Motoba *et al.* [13]. The errors in the spectrum of the upper part are inclusive of both the statistical and the acceptance contributions. Only major contributions are shown in the lower part with a common, arbitrary 1 MeV width, although each of the two bars in Fig. 3 between 25 and 27 MeV stands for ^{7}Be states spread over roughly $2-3$ MeV. The correspondence of the structures observed in the experimental spectra with the rates of decay to different excited states of the daugther nucleus, assuming initial spin-parity $1/2^+$, is clear. The peak structure corresponds to the production of ^{7}Be in its $3/2^-$ ground-state and in its only bound $1/2^-$ excited state, at 429 keV. Due to the FINUDA experimental resolution these close levels are not resolved and the gaussian fit superimposed on the data points yields a FWHM ~ 4.5 MeV, compatible with the intrinsic resolution of the apparatus: $\Delta T/T \sim 11\%$ FWHM at 38 MeV. The part of the spectrum at lower energies is due to three body decays, including also the point at ~ 31 MeV, located at $\sim 2.5\ \sigma$ from the peak center.

9

The portion of the spectrum that cannot be measured due to our experimental detection threshold (~ 22 MeV) is negligible if compared with the errors affecting the counts in the spectrum, according to the calculated excitation spectra shown in [13]. The same holds also for the other hypernuclei studied in this paper. It is then reasonable to compare the total area of the spectrum with the decay rates summed over the whole excitation energy interval, as done in the next section.

The shape of the spectrum confirms the spin assigned to the hypernuclear ground state of $^{7}_{\Lambda}$Li [32]. Indeed, only a spin-parity $1/2^+$ for $^{7}_{\Lambda}$Li ground state, shown by red bars, reproduces the fitted peak at ~ 36 MeV due to the ^{7}Be ground state and excited state at 429 keV. A spin-parity $3/2^+$ for $^{7}_{\Lambda}$Li ground state would imply a radically different spectrum shape [13,18], as indicated in Fig. 3 by the blue bars, short of any peak about ^{7}Be ground state and its 429 keV excited state.
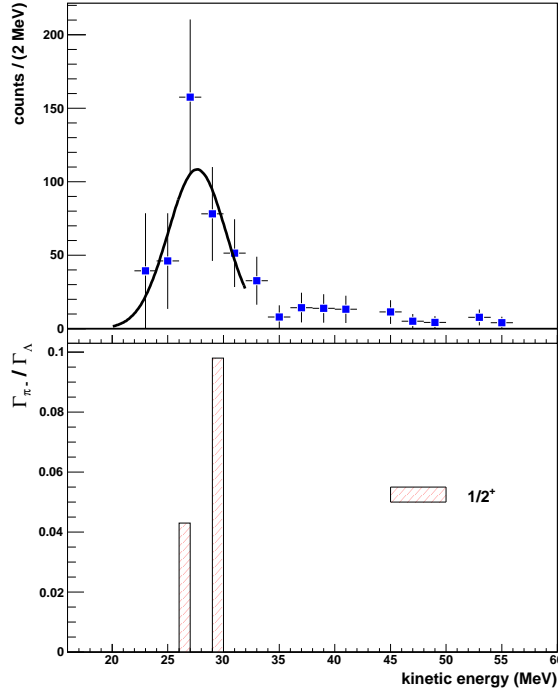
3.2. $^{9}_{\Lambda}$Be

Fig. 4. Upper part: kinetic energy spectrum of MWD π^- for $^{9}_{\Lambda}$Be after acceptance correction. The solid curve is a gaussian fit to the peak in the spectrum, to compare with theoretical predictions in the lower part. Lower part: calculated major decay rates to final ^{9}B states from [18], in red bars for $^{9}_{\Lambda}$Be ground-state spin-parity $1/2^+$.

In Fig. 4 the acceptance corrected spectrum for $^{9}_{\Lambda}$Be is shown in the upper part and compared with calculated decay ratios ($\Gamma_{\pi^-}/\Gamma_{\Lambda}$) to final ^{9}B states [18] shown in the lower part. The errors in the spectrum of the upper part are again inclusive of both the statistical and the acceptance contributions. Only major contributions are shown in the

10

lower part with a common, arbitrary 1 MeV width. In this case too, as for $^7_\Lambda$Li above, the calculated rates are very close to those calculated by Motoba *et al.* [13].

In the $^9_\Lambda$Be spectrum our energy resolution does not allow a separation between the two components predicted to dominate the spectrum [13,18], the ^{9}B ground-state $3/2^-$ and the excited state $1/2^-$ at 2.75 MeV. As a consequence, the gaussian fit superimposed on the data points yields a FWHM $\sim$ 7.5 MeV. The correspondence between the experimental spectrum and the calculated rates of decay to different excited states of the daugther nucleus is clear. Our spectrum confirms the interpretation from (π^+, K^+) reactions [25] according to which the $^9_\Lambda$Be ground state is dominantly a $1s$-Λ coupled to ^{8}Be(0^+) ground state.
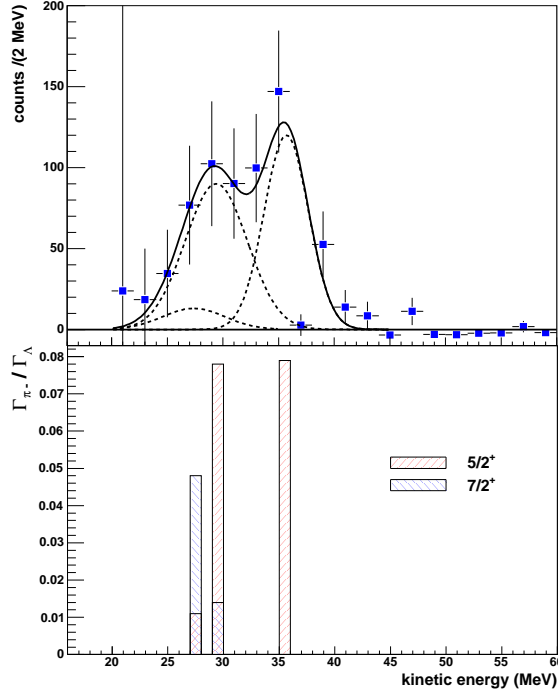
3.3. $^{11}_\Lambda$B

Fig. 5. Upper part: kinetic energy spectrum of MWD π^- for $^{11}_\Lambda$B after acceptance correction. The solid curve is a two-gaussian fit to the peaks in the spectrum, to compare with theoretical predictions in the lower part; dashed curves are the single components. Lower part: calculated major decay rates to final ^{11}C states from [18], in red bars for $^{11}_\Lambda$B ground-state spin-parity $5/2^+$, and in blue bars for $^{11}_\Lambda$B ground-state spin-parity $7/2^+$.

In Fig. 5 the spectrum for $^{11}_\Lambda$B is shown and compared with calculated decay rates to final ^{11}C states [18]. The errors in the spectra are again inclusive of both the statistical and the acceptance contributions. Major and secondary contributions are shown in the lower part with a common, arbitrary 1 MeV width. Assuming ground-state spin-parity $5/2^+$, it is possible to identify two major contributions in the $^{11}_\Lambda$B spectrum due to ^{11}C ground-state $3/2^-$ and its $7/2^-$ excited state at 6.478 MeV, both shown by red bars.

11

A third contribution due to the $3/2^-$ excited state at 8.10 MeV is considerably weaker than the former ones, its main effect being to introduce some asymmetry to the overall spectrum towards lower kinetic energies. Additional contribution of a similar strength [11] in this energy range arises from transitions to several sd states within $7 - 10$ MeV excitation energy in ^{11}C (not shown in Fig. 5). It is clear from the figure that the shape of the spectrum is well reproduced by assigning spin-parity $5/2^+$ to $^{11}_\Lambda$B$_{g.s.}$. Assuming ground-state spin-parity $7/2^+$, the ^{11}C ground-state peak is missing and the dominant decay is to the $5/2^-$ excited state at 8.420 MeV shown by a blue bar. A secondary contribution due to the $7/2^-$ excited state at 6.478 MeV is also considerably weaker than that arising under the assumption of spin-parity $5/2^+$. We note that the major contributions to the $^{11}_\Lambda$B spectrum discussed above for both $^{11}_\Lambda$B$_{g.s.}$ possible spin-parity values are also borne out by the calculation of Ref. [11].

A $5/2^+$ assignment for $^{11}_\Lambda$B ground-state, first made by Zieminska studying emulsion spectra [33], was experimentally confirmed by the KEK measurement [9] comparing the derived value of the total π^- decay rate with the total π^- decay rate calculated in [11]. However, it is the present measurement of both the decay spectrum shape and of the total π^- decay rate (see next section) that gives the first solid confirmation of $J^\pi(^{11}_\Lambda$B$_{g.s.}) = 5/2^+$.

3.4. $^{15}_\Lambda$N

In Fig. 6 the spectrum for $^{15}_\Lambda$N is shown and compared with calculated decay rates to final ^{15}O states [18]. The errors in the spectra are again inclusive of both the statistical and the acceptance contributions. In the experimental spectrum, the ^{15}O ground-state $1/2^-$ contribution stands out clearly, along with a secondary structure separated by about 6 MeV. The gaussian fit of the ground state component yields a FWHM of ~ 6 MeV, larger than our standard value ~ 4.5 MeV due to the already mentioned malfunctioning of the apparatus (see caption of Table 2) and to the limited statistics. The fit to the lower-energy secondary structure is strongly influenced by the substantial error affecting the lowest energy point. According to Refs. [12,18], this secondary structure derives most of its strength from sd states scattered around 6 MeV excitation while the contribution of the ^{15}O $p_{3/2}^{-1}p_{1/2}$ excited state at 6.176 MeV is negligible. We note that, in the upper part of Fig. 6, the bump at about 37 MeV kinetic energy might be caused by the reaction chain $K^- + {}^{16}$O $\to \pi^0 + \alpha + {}^{12}_\Lambda$B, $^{12}_\Lambda$B $\to \pi^- + {}^{12}$C$_{g.s.}$, with a non negligible pion charge exchange in the D$_2$O target. The points at ~ 42 MeV and ~ 46 MeV, figuring a $\sim 1.5\sigma$ statistical significance, are interpreted as mere statistical fluctuations.

The ground-state spin has not been determined experimentally. The most recent theoretical study of Λ-hypernuclear spin dependence [30] predicts $J^\pi(^{15}_\Lambda$N$_{g.s.}) = 3/2^+$, setting the $1/2^+$ excited ground-state doublet level about 90 keV above the $3/2^+$ ground-state. The spin ordering, however, cannot be determined from the γ-ray de-excitation spectra measured recently on a ^{16}O target at Brookhaven [34]. As for MWD, the prominence of ^{15}O$_{g.s.}$ in the spectrum of Fig. 6 supports this $J^\pi(^{15}_\Lambda$N$_{g.s.}) = 3/2^+$ theoretical assignment since the decay $^{15}_\Lambda$N$(1/2^+) \to \pi^- + {}^{15}O_{g.s.}$ is suppressed according to the following simple argument. Recent shell-model calculations suggest that the nuclear-core ^{14}N$_{g.s.}$ wavefunction is very close to a $^3D_1$ wavefunction [30], which for $J^\pi(^{15}_\Lambda$N$) = 1/2^+$ leads in the weak coupling limit to a single LS hypernuclear component $^4D_{1/2}$ for $^{15}_\Lambda$N. Since the
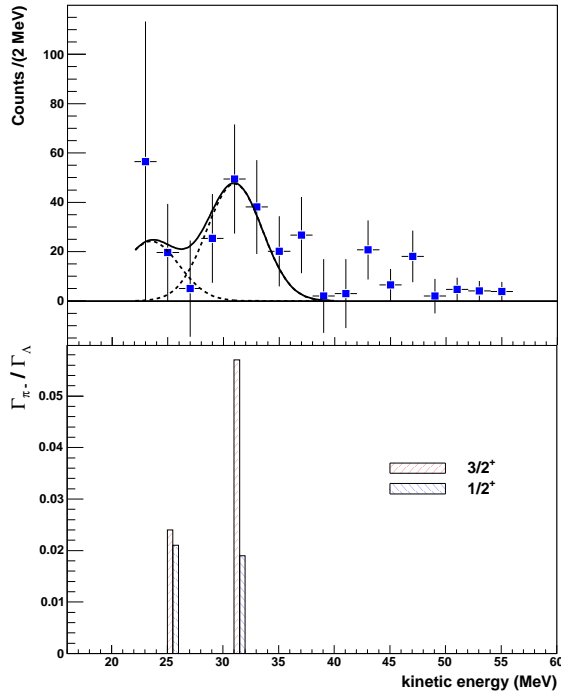
12

Fig. 6. Upper part: kinetic energy spectrum of MWD π^- for $^{15}_\Lambda$N after acceptance correction. The solid curve is a two-gaussian fit to the peaks in the spectrum, to compare with theoretical predictions in the lower part; dashed curves are the single components. Lower part: calculated major decay rates to final ^{15}O states from [18], in red bars for $^{15}_\Lambda$N ground-state spin-parity $3/2^+$, and in blue bars for $^{15}_\Lambda$N ground-state spin-parity $1/2^+$. Note that in this case the arbitrary bar width was reduced to 0.5 MeV to avoid overlap and to facilitate the comparison between the two spin hypotheses: indeed, the energies of the produced final states are practically the same.

transition $^{15}_\Lambda$N$(^4D_{1/2}) \rightarrow {}^{15}O(^2P_{1/2})$ requires spin-flip, it is forbidden for the dominant π^--decay s-wave amplitude. In a more realistic calculation, for spin-parity $3/2^+$, the ^{15}O ground-state main peak is expected to dominate over the secondary peak at about 6 MeV by a ratio close to 3:1, as shown in the lower part of Fig. 6 by the red bars [18]. This is in rough agreement with the fitted gaussians shown by dashed lines in the upper part of Fig. 6, where the relative contribution of the ^{15}O g.s. gaussian amounts to $(67 \pm 18)\%$. In contrast, for spin-parity $1/2^+$ the calculation in Ref. [18] produces a ratio close to 1:1 with respect to the ~ 6 MeV excitation, as shown by the blue bars in the lower part. Thus, the shape of the measured spectrum suggests that $J^\pi(^{15}_\Lambda$N$_{g.s.}) = 3/2^+$. [2]

4. MWD decay ratios and total decay rates

In general, due to the quite large errors affecting the spectra and to the lack of energy resolution at low values, the assignment of distinct MWD transitions to the daughter

---

[2] We note that the calculations in Refs. [12,13] suggest that neither the shape of the decay spectrum nor the total π^- decay rate of $^{15}_\Lambda$N are sensitive to the assumed value of the ground-state spin. However, it has been shown recently [18] that these older results for $^{15}_\Lambda$N violate a model-independent sum rule and, therefore, are not used here further to suggest interpretations of the present experimental results.

13

nucleus in our experimental spectra is somewhat tentative, except for the two-body component of $^7_\Lambda$Li. However, by considering complementarily the total area of each spectrum it is possible to infer decay rates with a reasonable statistical significance.

The branching ratios of the MWD reaction, $b_{\pi^-} = \Gamma_{\pi^-}/\Gamma_{tot}$, were evaluated for each hypernucleus as:

$$b_{\pi^-} = \frac{N_{\pi^--decay}}{N_{hyp}} \tag{12}$$

where $N_{\pi^--decay}$ is the number of the π^- MWD reactions and N_{hyp} is the number of the produced hypernuclei.

The number of MWD reactions was obtained from the counts in the momentum and the kinetic energy spectra after subtracting the residual background discussed in the previous section. In both cases, counts were considered up to the kinematical limit for a pure two-body decay, folded by our experimental resolution.

	$b_{\pi^-} = \Gamma_{\pi^-}/\Gamma_{tot}$	$\Gamma_{tot}/\Gamma_\Lambda$	$\Gamma_{\pi^-}/\Gamma_\Lambda$	previous data	theory
$^5_\Lambda$He	$0.323 \pm 0.062^{+0.025}_{-0.020}$	1.03 ± 0.08 [6] 0.947 ± 0.038 [23]	$0.332 \pm 0.069^{+0.026}_{-0.021}$ $0.306 \pm 0.060^{+0.025}_{-0.020}$	0.44 ± 0.11 [6] 0.340 ± 0.016 [23]	0.393 [10] 0.305 [18]
$^7_\Lambda$Li	$0.315 \pm 0.041^{+0.015}_{-0.012}$	1.12 ± 0.12 linear fit	$0.353 \pm 0.059^{+0.017}_{-0.013}$		0.304 [13] (0.179) 0.356 [18] (0.176)
$^9_\Lambda$Be	$0.154 \pm 0.040^{+0.011}_{-0.007}$	1.15 ± 0.13 linear fit	$0.178 \pm 0.050^{+0.013}_{-0.008}$		0.172 [13] 0.186 [18]
$^{11}_\Lambda$B	$0.199 \pm 0.039^{+0.041}_{-0.018}$	1.25 ± 0.08 [35] 1.37 ± 0.16 [37]	$0.249 \pm 0.051^{+0.051}_{-0.023}$	0.22 ± 0.05 [36] $0.23 \pm 0.06 \pm 0.03$ [8] $0.212 \pm 0.036 \pm 0.045$ [9]	0.213 [13] (0.116) [11] 0.196 [18] (0.101) [18]
$^{15}_\Lambda$N	$0.085 \pm 0.028^{+0.011}_{-0.010}$	1.26 ± 0.18 linear fit	$0.108 \pm 0.038^{+0.014}_{-0.013}$		0.090 [13] (0.074) [38] 0.080 [18] (0.040) [18]

Table 3

Branching ratios b_{π^-}, total hypernuclear weak decay rates $\Gamma_{tot}/\Gamma_\Lambda$ mostly from a linear fit in A, and total decay rates $\Gamma_{\pi^-}/\Gamma_\Lambda$ evaluated for charged MWD. Total decay rates are given in units of Γ_Λ. In the second and fourth columns the first quoted error is statistical, the second one is systematic. Comparison with previous measurements and theoretical predictions is reported. The calculated total rates are for ground state spin-parity $1/2^+$ for $^7_\Lambda$Li, $5/2^+$ for $^{11}_\Lambda$B and $3/2^+$ for $^{15}_\Lambda$N (in brackets $3/2^+$ for $^7_\Lambda$Li, $7/2^+$ for $^{11}_\Lambda$B and $1/2^+$ for $^{15}_\Lambda$N).

To evaluate the number of formed hypernuclei the area of the inclusive binding energy spectra was evaluated within the intervals reported in Table 1, after subtraction of the K^-np background and of the K^- in flight decay contribution, as described above.

14

The obtained values of the branching ratios, b_{π^-}, are reported in Table 3 with statistical and systematic errors. The latter ones are due to the different techniques used to evaluate the areas and the background in the inclusive spectra, while the systematic error due to the detection threshold of the apparatus has been estimated to be less than 2% and has been neglected. A preliminary account of the results presented here can be found in [39]. Total decay rates were calculated, using known $\Gamma_{tot}/\Gamma_\Lambda$ values or relying on a linear fit to the known values of all measured Λ-hypernuclei in the mass range $A = 4 - 12$ [32] as shown in Table 3:

$$\Gamma_{tot}/\Gamma_\Lambda(A) = (0.990 \pm 0.094) + (0.018 \pm 0.010) \cdot A, \quad \chi^2/ndf = 5.317/6. \tag{13}$$

A good agreement holds among the present results and previous measurements, when existing, and among the present results and theoretical calculations assuming ground state spins as listed in the caption. The calculated total decay rates for the other choice of ground state spins (in brackets) are substantially lower and disagree with the experimentally derived values. In particular, the total π^- decay rate of $^{15}_\Lambda$N and its decay spectrum shape, as evaluated here, agree with calculations by Motoba *et al.* [13] and by Gal [18] assuming a ground-state spin-parity assignment $3/2^+$. These two calculations disagree for a $1/2^+$ spin-parity assignment, but as argued in Section 3 (footnote) the new calculation [18] for $^{15}_\Lambda$N displays a higher level of consistency with the other species considered theoretically and in this sense it updates the older calculations [12,13]. The calculation by Gal [18] finds a significantly smaller total decay rate for $1/2^+$ spin-parity than for a $3/2^+$ spin-parity assignment, by $\sim 2\sigma$ lower than the rate evaluated by us as listed in the table. Furthermore, we recall that the measured spectrum shape looks similar to the one calculated for $3/2^+$ spin-parity, but only marginally to that evaluated in Ref. [18] for $1/2^+$ spin-parity. Therefore, based on a comparison between both our MWD spectrum shape and the evaluated decay rate and the calculation by one of the authors [18], the assignment $J^\pi(^{15}_\Lambda N_{g.s.}) = 3/2^+$ is made.

5. Conclusions

We have reported a systematic study of MWD of p-shell Λ-hypernuclei by the FINUDA experiment, performing for the first time a magnetic analysis of spectra of π^-'s from MWD of $^7_\Lambda$Li, $^9_\Lambda$Be, $^{11}_\Lambda$B and $^{15}_\Lambda$N. MWD decay rates $\Gamma_{\pi^-}/\Gamma_\Lambda$ have been evaluated and compared with previous measurements and theoretical calculations. The spin-parity assignments $J^\pi(^7_\Lambda Li_{g.s.}) = 1/2^+$ and $J^\pi(^{11}_\Lambda B_{g.s.}) = 5/2^+$ were confirmed and a new assignment, $J^\pi(^{15}_\Lambda N_{g.s.}) = 3/2^+$, was made based on the shape of the MWD spectra and the evaluated decay rates.

6. Aknowledgements

References

[1] R.H. Dalitz, *Phys. Rev.* **112** (1958) 605.
R.H. Dalitz, L. Liu, *Phys. Rev.* **116** (1959) 1312.

[2] R.H. Dalitz, *Nucl. Phys.* **41** (1963) 78.
D. Ziemińska, R.H. Dalitz, *Nucl. Phys.* **B 74** (1974) 248; *Nucl. Phys.* **A 238** (1975) 453.
D. Kiełczewska, D. Ziemińska, R.H. Dalitz, *Nucl. Phys.* **A 333** (1980) 367.

[3] D.H. Davis, *Nucl. Phys.* **A 754** (2005) 3c.

[4] H. Outa, *et al., Nucl. Phys.* **A 585** (1995) 109c.

[5] H. Outa, *et al., Nucl. Phys.* **A 639** (1998) 251c.

[6] J.J. Szymanski, *et al., Phys. Rev.* **C 43** (1991) 849.

[7] A. Sakaguchi, *et al., Phys. Rev.* **C 43** (1991) 73.

[8] H. Noumi, *et al., Phys. Rev.* **C 52** (1995) 2936.

[9] Y. Sato, *et al., Phys. Rev.* **C 71** (2005) 025203.

[10] T. Motoba, H. Bandō, T. Fukuda, J. Žofka, *Nucl. Phys.* **A 534** (1991) 597.

[11] H. Bandō, T. Motoba, J. Žofka, in *Perspectives of Meson Science*, Eds. T. Yamazaki, K. Nakai, K. Nagamine (North Holland, Amsterdam, 1992) pp. 571-660.

[12] T. Motoba, K. Itonaga, H. Bandō, *Nucl. Phys.* **A 489** (1988) 683.

[13] T. Motoba, K. Itonaga, *Progr. Theor. Phys. Suppl.* **117** (1994) 477.

[14] H. Bandō, H. Takaki, *Progr. Theor. Phys. Suppl.* **72** (1984) 109; *Phys. Lett.* **B 150** (1985) 409.

[15] E. Oset, L.L. Salcedo, *Nucl. Phys.* **A 443** (1985) 704; E. Oset, P. Fernández de Córdoba, L.L. Salcedo, R. Brockmann, *Phys. Rep.* **188** (1990) 79.

[16] E. Friedman, *et al., Phys. Rev.* **C 72** (2005) 034609, and references to earlier works therein.

[17] E. Friedman, A. Gal, *Phys. Rep.* **452** (2007) 89.

[18] A. Gal, π^- *decay rates of p-shell hypernuclei revisited*, arXiv:0904.1174v3 [nucl-th], *Nucl. Phys.* **A** (in press).

[19] M. Agnello, *et al., Phys. Lett.* **B 622** (2005) 35.

[20] M. Agnello, *et al., Nucl. Instr. Meth.* **A 570** (2007) 205.

[21] M. Agnello, *et al., Nucl. Phys.* **A 804** (2008) 151.

[22] M. Agnello, *et al., Phys. Rev. Lett.* **94** (2005) 212303.
M. Agnello, *et al., Nucl. Phys.* **A 775** (2006) 35.
M. Agnello, *et al., Phys. Lett.* **B 654** (2007) 80.
M. Agnello, *et al., Phys. Lett.* **B 669** (2008) 229.

[23] S. Kameoka, *et al., Nucl. Phys.* **A 754** (2005) 173c.

[24] M. Jurič, *et al., Nucl. Phys.* **B 52** (1973) 1.

[25] O. Hashimoto, *et al., Nucl. Phys.* **A 639** (1998) 93c;
O. Hashimoto, H. Tamura, *Prog. Part. Nucl. Phys.* **57** (2006) 564.

[26] M. Agnello, *et al.,* in *Hypernuclear and Strange Particle Physics, HYP2006*, Eds. J. Pochadzalla, Th. Walcher, SIF and Springer (2007) p. 57.

[27] H. Noumi, *et al., Nucl. Phys.* **A 691** (2001) 123c.

[28] P.H. Pile, *et al., Phys. Rev. Lett.* **66** (1991) 2585.

[29] H. Hotchi, *et al., Phys. Rev.* **C 64** (2001) 044302.

[30] D.J. Millener, *Nucl. Phys.* **A 804** (2008) 84.

[31] R.H. Dalitz, D.H. Davis, D.N. Tovee, *Nucl. Phys.* **A 450** (1986) 311c.

[32] J. Sasao, *et al., Phys. Lett.* **B 579** (2004) 258.

[33] D. Ziemińska, *Nucl. Phys.* **A 242** (1975) 461.

[34] M. Ukai, *et al., Phys. Rev.* **C 77** (2008) 054315.

[35] H. Park, *et al., Phys. Rev.* **C 61** (2000) 054004.

[36] A. Montwill, *et al., Nucl. Phys.* **A 234** (1974) 413.

[37] R. Grace, *et al., Phys. Rev. Lett.* **55** (1985) 1055.

[38] T. Motoba, private communication.

[39] M. Agnello, *et al.,* "Mesonic and Non-Mesonic Weak Decay of Hypernuclei with FINUDA", presented at PANIC08, Eilat, Israel, November 2008, to be published in *Nucl. Phys.* **A**.